Clim. Past Discuss., 11, 3699–3728, 2015
www.clim-past-discuss.net/11/3699/2015/
doi:10.5194/cpd-11-3699-2015

Climate of the Past Discussions
Open Access

A Late Pleistocene sea level stack

R. M. Spratt and L. E. Lisiecki

Department of Earth Science, University of California, Santa Barbara, USA

Received: 7 July 2015 – Accepted: 22 July 2015 – Published: 13 August 2015

Correspondence to: L. E. Lisiecki (lisiecki@geol.ucsb.edu)

Published by Copernicus Publications on behalf of the European Geosciences Union.

Abstract

Late Pleistocene sea level has been reconstructed from ocean sediment core data using a wide variety of proxies and models. However, the accuracy of individual reconstructions is limited by measurement error, local variations in salinity and temperature, and assumptions particular to each technique. Here we present a sea level stack (average) which increases the signal-to-noise ratio of individual reconstructions. Specifically, we perform principal component analysis (PCA) on seven records from 0–430 ka and five records from 0–798 ka. The first principal component, which we use as the stack, describes ∼ 80 % of the variance in the data and is similar using either five or seven records. After scaling the stack based on Holocene and Last Glacial Maximum (LGM) sea level estimates, the stack agrees to within 5 m with isostatically adjusted coral sea level estimates for Marine Isotope Stages 5e and 11 (125 and 400 ka, respectively). When we compare the sea level stack with the δ^{18}O of benthic foraminifera, we find that sea level change accounts for about ∼ 40 % of the total orbital-band variance in benthic δ^{18}O, compared to a 65 % contribution during the LGM-to-Holocene transition. Additionally, the second and third principal components of our analyses reflect differences between proxy records associated with spatial variations in the δ^{18}O of seawater.

1 Introduction

Glacial–interglacial cycles of the Late Pleistocene (0–800 ka) produced sea level changes of as much as 130 m, primarily associated with the growth and retreat of continental ice sheets. Precise and accurate reconstructions of sea level change during these cycles are important both for understanding the mechanisms responsible for 100 ka glacial cycles and for quantifying the amplitude and rate of ice sheet responses to climate change. Sea level estimates for warm interglacials at 125 and 400 ka are of particular interest as potential analogs for future sea level rise (Kopp et al., 2009;

CPD
11, 3699–3728, 2015

Raymo and Mitrovica, 2012). Nearly continuous coral elevation data have generated well-constrained sea level reconstructions since the Last Glacial Maximum (LGM) at 21 ka (Clark et al., 2009; Lambeck et al., 2014). However, beyond the LGM sea level estimates from corals are discontinuous and have relatively large age uncertainties (e.g., Thompson and Goldstein, 2005; Medina-Elizalde, 2013). Several techniques have been developed to generate longer continuous sea level reconstructions from marine sediment core data. Each of these techniques is subject to different assumptions and regional influences. Here, we identify the common signal present in seven Late Pleistocene sea level records as well as some of their differences.

These sediment core records convert $\delta^{18}O_c$, the oxygen isotope content of the calcite tests of foraminifera, to sea level using one of several techniques. In three records, temperature proxies were used to remove the temperature-dependent fractionation effect from $\delta^{18}O_c$ in order to solve for the $\delta^{18}O$ of seawater ($\delta^{18}O_{sw}$). Other techniques for transforming $\delta^{18}O_c$ to sea level include the polynomial regression of $\delta^{18}O_c$ to coral-based sea level estimates, hydraulic control models of semi-isolated basins, and inverse models of ice volume and temperature. Each of these techniques produce slightly different results for a variety of reasons. For example, $\delta^{18}O_{sw}$ varies spatially due to differences in water mass salinity and deep water formation processes (Adkins et al., 2002). Reconstructions also vary based on sensitivity to eustatic vs. relative sea level (RSL) and temporal resolution.

Principal component analysis (PCA) is used to identify the common sea level signal in these seven records (i.e., to produce a sea level "stack") and to evaluate differences between reconstruction techniques. By combining multiple sea level records with different underlying assumptions and sources of noise, the sea level stack has a higher signal-to-noise ratio than the individual sea level records used to construct it.

CPD
11, 3699–3728, 2015

2 Sea level reconstruction techniques

2.1 Coral proxies

Corals provide the most prominent sea level proxy, but the accuracy of coral sea level reconstructions varies based on the availability, condition and age of corals. Coral sea level is especially accurate between 0–21 ka because of nearly continuous pristine coral specimens from several locations during this time period (e.g., Clark et al., 2009; Medina-Elizalde, 2013). However, coral data is increasingly discontinuous and inaccurate prior to 21 ka due to difficulty finding pristine and in situ older corals (particularly during sea level lowstands) and due to U-Th age uncertainties in older corals caused by isotope free exchange with the surrounding environment (e.g., Thompson and Goldstein, 2005; Medina-Elizalde, 2013). Interpretation of sea level from corals often requires a correction for rates of continental uplift, which may not be known precisely. Glacial isostatic adjustment and species habitat depth (up to 6 m below sea level) may also affect sea level estimates (Raymo and Mitrovica, 2012; Medina-Elizalde, 2013). Wave destruction and climate variations also alter coral growth patterns and may affect the height of colonies relative to sea level (Medina-Elizalde, 2013).

2.2 Seawater $\delta^{18}O$

Global ice volume is a main control on the global mean of $\delta^{18}O$ in seawater ($\delta^{18}O_{sw}$). Global mean $\delta^{18}O_{sw}$ is estimated to decrease by 0.008 to 0.01 ‰ m^{-1} of sea level rise (Adkins et al., 2002; Elderfield, 2012; Shakun et al., 2015). However, $\delta^{18}O_{sw}$ also varies spatially based on patterns of evaporation and precipitation and deep water formation processes. The $\delta^{18}O$ of calcite ($\delta^{18}O_c$) is affected both by the $\delta^{18}O_{sw}$ and temperature. In the absence of any post-depositional alteration, subtracting the temperature-dependent fractionation effect from $\delta^{18}O_c$ (Shackleton, 1974) should yield a good estimate of the $\delta^{18}O_{sw}$ in which the calcite formed. The $\delta^{18}O_c$ of benthic foraminifera reflects the temperature and $\delta^{18}O_{sw}$ of deep water, while the $\delta^{18}O_c$ of planktonic

CPD
11, 3699–3728, 2015

foraminifera is affected by sea surface temperature (SST) and the $\delta^{18}O_{sw}$ of near-surface water.

2.3 Benthic $\delta^{18}O_{sw}$

Our analysis includes two benthic $\delta^{18}O_{sw}$ records from the North Atlantic and South Pacific, which use the Mg/Ca ratio of benthic foraminifera as a temperature proxy. The South Pacific benthic $\delta^{18}O_{sw}$ record (Elderfield et al., 2012) comes from Ocean Drilling Program (ODP) site 1123 (171° W, 41° S, 3290 m). This site reflects the properties of Lower Circumpolar Deep Water, which is a mix of Antarctic Bottom Water (AABW) and North Atlantic Deep Water (NADW). Mg/Ca ratios and $\delta^{18}O_c$ were determined from separate samples of the same species of *Uvigerina,* which is considered fairly insensitive to the deep water carbonate saturation state (Elderfield et al., 2012). Elderfield et al. (2012) interpolate their data to 1 ka spacing, perform a 5 ka Gaussian smoothing, and convert from $\delta^{18}O_{sw}$ to sea level using a factor of 0.01 ‰ m^{-1}. Measurement uncertainties for temperature and $\delta^{18}O_c$ generate a $\delta^{18}O_{sw}$ uncertainty of ±0.2 ‰, corresponding to bottom water temperature range of ±1 °C or about 22 m of sea level.

The North Atlantic $\delta^{18}O_{sw}$ reconstruction is from Deep Sea Drilling Program (DSDP) site 607 (32° W, 41° N, 3427 m) and nearby piston core Chain 82-24-23PC (Sosdian and Rosenthal, 2009). These sites are bathed by NADW today but were likely influenced by AABW during glacial maxima (Raymo et al., 1990). Mg/Ca was measured using two benthic foraminiferal species, *Cibicidoides wuellerstorfi* and *Oridorsalis umbonatus,* which may be affected by changes in carbonate ion saturation state, particularly when deep water temperature drops below 3 °C (Sosdian and Rosenthal, 2009). The $\delta^{18}O_c$ data come from a combination of *Cibicidoides* and *Uvigerina* species. Sea level was estimated from benthic $\delta^{18}O_{sw}$ using a conversion of 0.01 ‰ m^{-1} and then taking a 3-point running mean. Combining the reported uncertainties for temperature (±1.1 °C) and $\delta^{18}O_c$ (±0.2 ‰) yields a sea level uncertainty of approximately ±20 m (one standard error) for the 3-point running mean.

CPD
11, 3699–3728, 2015

2.4 Planktonic $\delta^{18}O_{sw}$

A 49-core global stack uses the $\delta^{18}O_c$ from planktonic foraminifera paired with SST proxies from the same core. The planktonic species in this reconstruction were: *G ruber*, *G bulloides*, *G inflata*, *G sacculifer*, *N dutretriei*, and *N pachyderma*. Forty-four records span the most recent glacial cycle, and seven records extend back to 798 ka. Thirty-four records use Mg/Ca temperature estimates, and fifteen use the alkenone $U^{k'}_{37}$ temperature proxy. Because $U^{k'}_{37}$ measurements derive from coccolithophore rather than foraminifera, there is some chance the temperature measured may differ slightly from that affecting $\delta^{18}O_c$ (Schiebel et al., 2004). However, Shakun et al. (2015) observed no significant differences in $\delta^{18}O_{sw}$ estimated from the two SST proxies. An additional concern is that the surface ocean is affected by greater hydrologic variability and characterizes a smaller ocean volume than the deep ocean. Thus, planktonic $\delta^{18}O_{sw}$ may differ more from ice volume changes than benthic data. However, these potential disadvantages of using planktonic records may be largely compensated by the use of a global planktonic stack.

The first principal component (stack) of the planktonic records spanning the last glacial cycle represents 71 % of the variance in the records ($n = 44$), suggesting a strong common signal in planktonic $\delta^{18}O_{sw}$. However, the 800 ka planktonic $\delta^{18}O_{sw}$ stack appears to contain linear trends that differ from other sea level estimates. Therefore, Shakun et al. (2015) corrected their sea level estimate by detrending planktonic $\delta^{18}O_{sw}$ based on differences between planktonic and benthic $\delta^{18}O_c$. Standard errors in the $\delta^{18}O_{sw}$ stack increase from 0.05 ‰ for the last glacial cycle to 0.12 ‰ at 800 ka due to the reduction in the number of records. The equivalent sea level uncertainties are ±6 and ±18 m (1σ), respectively. All data were interpolated to even 3 ka time intervals.

CPD
11, 3699–3728, 2015

2.5 Benthic $\delta^{18}O_c$ – coral regression

The sea level reconstruction of Waelbroeck et al. (2002) was developed by fitting polynomial regressions between benthic $\delta^{18}O_c$ from North Atlantic cores NA 87-22/25 (55° N, 15° W, 2161 and 2320 m) and equatorial Pacific core V19-30 (3° S, 83° W, 3091 m) to sea level estimates for the last glacial cycle, primarily from corals. Quadratic polynomials were fit during times of ice sheet growth and during the glacial termination in the North Atlantic whereas a linear regression was fit to the Pacific glacial termination. A composite sea level curve was created from the most reliable sections of several cores, primarily from the Pacific. The composite time series was interpolated to an even 1.5 ka time window, and the uncertainty associated with this technique is estimated to be ±13 m of sea level.

2.6 Inverse ice volume model

The inverse model of Bintanja et al. (2005) is based on the concept that Northern Hemisphere (NH) subpolar surface air temperature plays a key role in determining both ice sheet size and deepwater temperature, which are the two dominant factors affecting benthic $\delta^{18}O_c$. A three-dimensional thermomechanical ice sheet model simulates ice sheet $\delta^{18}O$ content, height, and volume for NH ice sheets (excluding Greenland) as forced by subpolar air temperature, orbital insolation, and the modern spatial distributions of temperature and precipitation. Antarctic and Greenland ice sheets are assumed to account for 5 % of ocean isotopic change and 15 % of sea level change. Deep water temperature is assumed to scale linearly with the 3 ka mean air temperature. At each time step air temperature is adjusted to maximize agreement between predicted $\delta^{18}O_c$ and the observed value 0.1 ka later in a benthic $\delta^{18}O_c$ stack (Lisiecki and Raymo, 2005). The model solves for ice volume, temperature, and sea level changes since 1070 ka in 0.1 ka time steps; however, the $\delta^{18}O_c$ stack used to constrain the model has a resolution of 1–1.5 ka. Uncertainty in modeled sea level is approximately ±12 m (1σ).

CPD
11, 3699–3728, 2015

2.7 Hydraulic control models of semi-isolated basins

Two sea level reconstructions use hydraulic control models to relate planktonic $\delta^{18}O_c$ from the Red Sea and Mediterranean Sea to relative sea level. In these semi-isolated basins, $\delta^{18}O_{sw}$ is strongly affected by evaporation and exchange with the open ocean as affected by relative sea level at the basin's sill.

Red Sea RSL (Rohling et al., 2009) from 0–520 ka is estimated using the $\delta^{18}O_c$ of planktonic foraminifera from the central Red Sea (GeoTü-KL09). Because extremely saline conditions killed foraminifera during MIS 2 and MIS 12, $\delta^{18}O_c$ data for these time intervals were estimated by transforming bulk sediment values. Sea level is estimated using a physical circulation model for the Red Sea combined with an oxygen isotope model (Siddall et al., 2004). The physical circulation model simulates exchange flow through the Bab-el-Mondab strait which depends strongly on sea level. The current sill depth is 137 m, and its estimated uplift rate is 0.2 m ka^{-1}. The isotope model assumes steady state with exchange through the sill and evaporation/precipitation. Assumptions of the isotope model include: (1) modern evaporation rates and humidity, (2) open ocean $\delta^{18}O_{sw}$ scales as 0.01 ‰ m^{-1}, and (3) SST scales linearly with sea level. A 5 °C change in SST between Holocene and LGM is used to optimize the model's LGM sea level estimate. Steady state model solutions for different sea level estimates are used to develop a conversion between $\delta^{18}O_c$ and sea level, which is approximated as a fifth-order polynomial. Sensitivity tests using plausible ranges of climatic values yield a 2σ uncertainty estimate of ±12 m.

A Mediterranean RSL record (Rohling et al., 2014) is derived from a hydraulic model of flow through the Strait of Gibraltar (Bryden and Kinder, 1991) combined with evaporation and oxygen isotope fractionation equations for the Mediterranean (Rohling et al., 2004). Runoff and precipitation are parameterized based on present-day observations, humidity is assumed constant, and temperature is assumed to covary with sea level. The $\delta^{18}O_{sw}$ of Atlantic inflow is scaled using 0.009 ‰ m^{-1}, and net heat flow through the sill is assumed to be zero. The combined models yield a converter between $\delta^{18}O_c$

CPD
11, 3699–3728, 2015

and sea level, which is approximated as a polynomial. This polynomial conversion is applied to an eastern Mediterranean planktonic $\delta^{18}O_c$ stack (Wang et al., 2010) after identification and removal of sapropel layers. Model uncertainty is evaluated using random parameter variations, which yield 95 % confidence intervals of ±20 m for individual $\delta^{18}O_c$ values. In a probabilistic assessment of the final sea level reconstruction with 1 ka time steps these uncertainties are reduced to ±6.3 m. Additionally, the authors propose that RSL at this location is linearly proportional to eustatic sea level.

3 Methods

3.1 Age models

To create an average (or stack) of sea level records, all of the time series must be placed on a common age model (Fig. 1). Here we use the age model of the orbitally tuned "LR04" benthic $\delta^{18}O_c$ stack (Lisiecki and Raymo, 2005). Because the LR04 age model has an uncertainty of 4 ka in the Late Pleistocene, our interpretation focuses on the amplitude of sea level variability rather than its precise timing.

We do not assume that sea level varies synchronously with benthic $\delta^{18}O_c$. Rather, our age model development involved either aligning individual $\delta^{18}O_c$ to the LR04 $\delta^{18}O_c$ stack or aligning individual sea level records to other sea level records that had been placed on the LR04 age model based on $\delta^{18}O_c$ alignments. All alignments were performed using the Match graphic correlation software package (Lisiecki and Lisiecki, 2002). The benthic $\delta^{18}O_c$ records from sites 1123 and 607 were aligned to the LR04 stack. Similarly, the published age model for the planktonic $\delta^{18}O_{sw}$ stack was developed by aligning each core's benthic $\delta^{18}O_c$ record (or planktonic $\delta^{18}O_c$ where benthic data were unavailable) to the LR04 stack. The original age model of Bintanja et al. (2005) is also consistent with the LR04 age model because the LR04 stack was used as a constraint for the inverse model.

CPD
11, 3699–3728, 2015

However, for three reconstructions (Waelbroeck et al., 2002; Rohling et al., 2009, 2014) we aligned the individual sea level records with a preliminary sea level stack based on the other four sea level records on the LR04 age model. This was necessary because the local $\delta^{18}O_c$ signals in semi-isolated basins (Rohling et al., 2009, 2014) differ substantially from global mean benthic $\delta^{18}O_c$. In the coral-regression reconstruction, Waelbroeck et al. (2002) pasted together portions of individual cores to form a preferred global composite. Although each core has benthic $\delta^{18}O_c$ data, generating new age estimates for these cores could alter their $\delta^{18}O_c$ regression functions or create gaps or inconsistencies in the composite. The procedure of aligning these three sea level records (Waelbroeck et al., 2002; Rohling et al., 2009, 2014) to a preliminary sea level stack should be approximately as accurate as the $\delta^{18}O_c$ alignments. However, the direct sea level alignments do have a slightly greater potential to align noise or local sea level variability.

After age models were adjusted, five of the records ended within the Holocene. Therefore, we appended a value of 0 m (i.e., present day sea level) at 0 ka. In the two records which did end at 0 ka, modern sea level estimates were slightly below zero: −1.5 m (Bintanja, 2005) and −1.3 m (Rohling et al., 2014).

3.2 Principal component analysis

We use both relative and eustatic sea level estimates in the Principal Component Analysis (PCA) because PCA should identify the common variance that dominates both relative and eustatic sea level records. Three records are proxies for relative sea level at their respective locations: the strait of Gibraltar (Rohling et al., 2014), the Bab el Mondab strait (Rohling et al., 2009), and tropical coral terraces (Waelbroeck et al., 2002). The inverse model generates eustatic sea level from a modeled ice volume estimate (Bintanja et al., 2005), and the three $\delta^{18}O_{sw}$ records (Elderfield et al., 2012; Sosdian and Rosenthal, 2009; Shakun et al., 2015) were scaled to eustatic sea level. However, for the planktonic stack we use the $\delta^{18}O_{sw}$ record rather than the eustatic sea

CPD
11, 3699–3728, 2015

level conversion because the sea level conversion involved detrending to make planktonic $\delta^{18}O_c$ values agree with benthic $\delta^{18}O_c$. Because PCA is designed to identify the common variance between the sea level proxies, it is preferable to keep the planktonic and benthic $\delta^{18}O_{sw}$ records independent of one another.

In the Mediterranean RSL record we removed putative sapropel layers at 434–452, 543–558, and 630–663 ka as visually identified by Rohling et al. (2014) and linearly interpolated across these gaps (Fig. 1). Although interpolation across large gaps is not ideal, we must assume some sea level value at these times in order to include this record in the PCA.

Before PCA, all seven records were interpolated to an even 1 ka time step. Then, to ensure equal weighting for each record in the PCA, each time series was normalized to a mean of zero and a standard deviation of one within each of the two time windows (0–430 and 0–798 ka). PCA was performed on seven records from 0–430 ka and five records from 0–798 ka (Fig. 2). Because PC1 produces similar loadings for each record (Table 1), the PC1 scores approximate the average of all records for each point in time, which we refer to as a sea level stack.

We scaled the short and long stacks to eustatic sea level using an LGM value of −130 m at 24 ka based on a GIA-corrected coral compilation (Clark et al., 2009) and a Holocene value of 0 m at 5 ka. We scale the Holocene at 5 ka because eustatic sea level has been essentially constant for the past 5 ka (Clark et al., 2009), whereas the sea level stacks display a trend throughout the Holocene perhaps due to bioturbation in the sediment cores. Scaling the sea level stack based on the mid-Holocene (rather than 0 ka) should more accurately correct for the effects of bioturbation on previous interglacials because those highstand values have been subjected to mixing from both above and below. Finally, a composite sea level stack was created by joining the 0–430 ka stack with the 431–798 ka portion of the long stack after each was scaled to sea level. Because the two scaled sea level stacks produce similar values for 0–430 ka (Fig. 2), no correction was needed to combine the records.

CPD
11, 3699–3728, 2015

4 Mean sea level estimates

Because each of the records in the PCA is a sea level proxy and PC1 describes the majority of variance in the records, PC1 should represent the underlying common eustatic sea level signal in all proxies. PC1 describes 82 % of the variance in the seven records from 0–430 ka and 76 % of proxy variance from 0–798 ka. Where the two time windows overlap (Fig. 2), the scaled sea level stacks have a root mean square error of only 3.4 m, thereby suggesting that the long stack is nearly as accurate as the short stack although it contains two fewer records.

To test the effectiveness of using the scaled PC1 as a record of mean sea level, we compared our stack with highstand and lowstand values identified from individual records and with coral-based estimates where available (Tables 2 and 3). We picked the relevant highstand or lowstand for each individual record by choosing the peak that lies within the age range of each Marine Isotope Stage (MIS) as identified in the sea level stack. Highstand or lowstand peaks which occurred outside of the age range of each particular glacial or interglacial stage were not used (e.g., extreme values at ~ 250 ka from sites 1123 and 607).

Highstand sea level estimates vary widely between individual records with standard deviations of 11–26 m for each isotopic stage (Table 3). For example, individual estimates for Marine Isotope Stage (MIS) 11 at ~ 400 ka vary between −1 to 57 m above modern, with a mean of 20 m and a standard deviation of 26 m. MIS 5e (119–126 ka) estimates range from −6 to 28 m above modern with a mean of 9 m and a standard deviation of 12 m. Generally, the highstand means have slightly greater amplitudes than our scaled stack; for example, the scaled stack estimates are 16 and 3 m for MIS 11 and MIS 5e, respectively. On the other hand, the mean of individual lowstands for the LGM (−121 m) underestimates eustatic sea level change, which is estimated to be −125 to −134 m (Clark et al., 2009; Lambeck et al., 2014; Rohling et al., 2014).

The means of the individually picked highstands may be biased by the additive effects of noise. Conversely, the stack may underestimate sea level highstands if the individual

CPD
11, 3699–3728, 2015

age models are not properly aligned. The most definitive sea level estimates come from GIA-corrected coral compilations, which yield highstand estimates of 6–13 m above modern for MIS 11 (Raymo and Mitrovica, 2012) and 8–9.4 m for MIS 5e (Kopp et al., 2009). These values suggest that the stack may be more accurate for MIS 11 than MIS 5e, potentially because age model uncertainty would have less effect on the longer MIS 11 highstand. In contrast, MIS 5e may have consisted of two highstands each lasting only ~ 2 ka separated by several thousand years with sea level at or below modern (Kopp et al., 2013). Thus, the stack's highstand estimates likely fail to capture short-term sea level fluctuations but rather reflect mean sea level during each interglacial.

5 The sea level contribution to benthic $\delta^{18}O_c$

The sea level stack and the LR04 benthic $\delta^{18}O_c$ stack are strongly correlated ($r = -0.90$). However, because $\delta^{18}O_c$ contains both an ice volume and temperature component, the $\delta^{18}O_c$ record has a greater amplitude than the ice volume-driven $\delta^{18}O_{sw}$ record. The spectral variance of $\delta^{18}O_{sw}$ and $\delta^{18}O_c$ in each orbital band can be used to determine the relative contributions of sea level and temperature variability in $\delta^{18}O_c$. For this comparison, we convert the sea level stack to $\delta^{18}O_{sw}$ using 0.009 ‰ m^{-1}.

Although some studies have used 0.01 ‰ m^{-1} (e.g., Sosdian et al., 2009; Elderfield et al., 2012; Rohling et al., 2009), this conversion factor is likely too high for global mean $\delta^{18}O_{sw}$ change at the LGM. Several lines of evidence suggest an LGM $\delta^{18}O_{sw}$ change of 1–1.1 ‰ (Duplessy et al., 2002; Adkins et al., 2002; Elderfield et al., 2012; Shakun et al., 2015), while LGM sea level was likely 125–134 m below modern (Clark et al., 2009; Lambeck et al., 2014; Rohling et al., 2014). These estimates suggest a conversion factor between 0.008–0.009 ‰ m^{-1}. A conversion of 0.008 ‰ m^{-1} would be consistent with a $\delta^{18}O_{ice}$ of −32 ‰ (Elderfield et al., 2012), similar to estimates for the Laurentide and Eurasian ice sheets (Duplessy et al., 2002; Bintanja et al., 2005; Elderfield et al., 2012). Therefore, 0.009 ‰ m^{-1} may be more appropriate when also

CPD
11, 3699–3728, 2015

considering changes in Greenland and Antarctic ice. However, the conversion factor between sea level and mean $\delta^{18}O_{sw}$ also likely varies through time as a result of changes in the mean isotopic content of each ice sheet (Bintanja et al., 2005) and their relative sizes.

Spectral analysis shows strong 100 and 41 ka peaks in both the LR04 benthic $\delta^{18}O_c$ stack and the sea level stack (Fig. 3). When converted to $\delta^{18}O_{sw}$, the sea level stack contains 44 % as much 100 ka power (using a frequency band of 0.009–0.013ka^{-1}) as benthic $\delta^{18}O_c$ and 33 % as much 41 ka power (0.024–0.026ka^{-1}). Considering all frequencies less than 0.1ka^{-1}, $\delta^{18}O_{sw}$ explains 41 % of the variance in $\delta^{18}O_c$. Therefore, we conclude that on average about 40 % of the glacial cycle variance in benthic $\delta^{18}O_c$ derives from ice volume change and 60 % from deep sea temperature change.

This $\sim$ 40 % ice volume contribution to benthic $\delta^{18}O_c$ is smaller than the contribution estimated across the LGM to Holocene transition. An LGM sea level change of 130 m (Clark et al., 2009) should shift mean $\delta^{18}O_{sw}$ by 1.17 ‰, whereas benthic $\delta^{18}O_c$ changed by 1.79 ‰ (Lisiecki and Raymo, 2005), suggesting that 65 % of the LGM $\delta^{18}O_c$ change was driven by ice volume. Many other studies have similarly found that the ice volume ($\delta^{18}O_{sw}$) contribution to $\delta^{18}O_c$ is greatest during glacial maxima (Bintanja et al., 2005; Elderfield et al., 2012; Rohling et al., 2014; Shakun et al., 2015). Additionally, the $\delta^{18}O_{sw}$ contribution varies by location, ranging from 0.7 to 1.37 ‰ based on glacial pore water reconstructions (Adkins et al., 2002). The wide variability in $\delta^{18}O_{sw}$ between sites suggests that changes in deep water formation processes (e.g., evaporation vs. brine rejection) greatly affect the $\delta^{18}O_{sw}$ signal regionally or locally. Therefore, the $\delta^{18}O_{sw}$ at a single site may differ considerably from eustatic sea level.

CPD
11, 3699–3728, 2015

6 Converting from benthic $\delta^{18}O_c$ and sea level

Although ice volume change accounts for only 40–65 % of benthic $\delta^{18}O_c$ change, many studies have used benthic $\delta^{18}O_c$ as a proxy for ice volume based on the argument that temperature and ice volume should be highly correlated through time (e.g., Imbrie and Imbrie, 1980; Abe-Ouchi et al., 2013). However, over the course of a glacial cycle the relative contributions of ice volume and temperature change dramatically, and temperature change precedes ice volume change (Bintanja et al., 2005; Elderfield et al., 2012; Shakun et al., 2015). Despite these complications the LR04 benthic $\delta^{18}O_c$ stack is strongly correlated with the sea level stack ($r = -0.9$). Here we explore more closely the functional relationship between benthic $\delta^{18}O_c$ and sea level as inspired by Waelbroeck et al. (2002).

Waelbroeck et al. (2002) solved for regression functions between several benthic $\delta^{18}O_c$ records and coral elevation data over the last glacial cycle and found different functional forms for glaciation vs. deglaciation and for the North Atlantic vs. equatorial Pacific $\delta^{18}O_c$. Here we compare the LR04 global benthic stack with the sea level stack from 0–798 ka. One advantage of this comparison is that both records use the same age model. We evaluate whether a single regression can be used for the Late Pleistocene and identify a potential change in the relationship between benthic $\delta^{18}O_c$ and sea level at ~ 400 ka.

One difference between the two stacks is that the sea level stack is smoother (Fig. 2), likely because some of the sea level records are low resolution and all records were interpolated to 1 ka spacing for PCA. Smoothing the LR04 stack using a 7 ka running mean improves the correlation between benthic $\delta^{18}O_c$ and sea level from -0.90 to -0.92. Next we apply a 2 ka lag to the smoothed LR04 stack, which improves the correlation to -0.94. OLS linear regression between the smoothed and lagged LR04 benthic $\delta^{18}O_c$ stack (x) and sea level in meters (h) yields the equation

$$h = -72.5x + 249.1 \quad (1)$$

CPD
11, 3699–3728, 2015

(Fig. 4, black line). The root mean square error (rmse) for this model is 10.5 m, but the fit is better for the older portion of the record (398–798 ka, rmse = 9.7 m) than the more recent portion (0–397 ka, rmse = 11.3 m). In particular, the linear model estimates sea levels that are 10–20 m too high during most highstands and lowstands back to MIS 10 at ~ 345 ka. A plot of sea level vs. the smoothed and lagged benthic $\delta^{18}O_c$ (Fig. 4b) suggests that the relationship between the two is approximately quadratic

$$h = -26x^2 + 135x - 162 \quad (2)$$

from 0–397 ka (rmse = 9.5 m) and linear from 398–798 ka. This transition appears to take place between 360–400 ka because MIS 11 clearly falls on the linear trend (Fig. 4c) whereas MIS 10 is much better fit by the quadratic (Fig. 4b). Because this transition occurs after MIS 11, the extreme duration or warmth of this interglacial might have played an important role in the transition.

A change in the relationship between benthic $\delta^{18}O_c$ and sea level could be caused by a change in the mean isotopic content of ice sheets or the relationship between ice volume and deep water temperature (possibly also global surface temperature). To explain this transition, interglacials after MIS 11 were likely warmer or had more depleted $\delta^{18}O_{sw}$ relative to ice volume. Similarly, glacial maxima were probably warmer and/or had less $\delta^{18}O_{sw}$ change. Combined changes in temperature and isotopic fractionation may be the most likely explanation since warmer ice sheets also probably have less depleted $\delta^{18}O_{ice}$. In fact Antarctic ice cores are isotopically less depleted during MIS 5e and MIS 9 than MIS 11 (Jouzel et al., 2010). Additionally, Antarctic surface temperatures and CO_2 levels were similar for all three interglacials (Masson-Delmotte et al., 2010; Petit et al., 1999) despite the smaller ice volume during MIS 11.

There is little direct evidence to explain the changing relationship between $\delta^{18}O_c$ and sea level during in glacial maxima because glacial values for both deep water temperature and the isotopic composition of Antarctic ice are similar throughout the last 800 ka. The change in glacial maxima after 400 ka could be caused by less depleted $\delta^{18}O_{ice}$ in Northern Hemisphere (NH) ice sheets. Although no long records of NH $\delta^{18}O_{ice}$ exist,

CPD
11, 3699–3728, 2015

global mean SST was 0.5–1 °C warmer during MIS 2, 6, and 8 than during MIS 12 (Shakun et al., 2015). Alternatively, the apparent linear trend between sea level and $\delta^{18}O_c$ during glacial maxima before 400 ka (Fig. 4c) could be an artifact of poor sea level estimates for MIS 12 and 16, which may be biased 10–20 m too high (Table 2) by interpolation across sapropel intervals in the Mediterranean RSL record (Rohling et al., 2014).

In conclusion, a systematic relationship can be defined between Late Pleistocene benthic $\delta^{18}O_c$ and sea level, and the functional form of this relationship likely changed after MIS 11. Change in the $\delta^{18}O_c$-sea level relationship during interglacials likely results from warmer high latitudes with less depleted $\delta^{18}O_{ice}$ after 400 ka. Glacial maxima after 400 ka may also have been warmer with less depleted NH $\delta^{18}O_{ice}$, but this apparent change during glacial maxima could be an artifact of bias in the sea level stack during MIS 12 and 16. Changes in the relationship between benthic $\delta^{18}O_c$ and sea level are also likely to have occurred during the early or mid-Pleistocene. For example, the same regression probably would not apply to the 41 ka glacial cycles of the early Pleistocene (Tian et al., 2003).

7 Differences between sea level proxies

Whereas PC1 tells us about the common variance between the sea level proxies, PC2 and PC3 tell us about their differences. PC2 represents 6 and 8 % of the variance for the short and long time windows, respectively. The scores and loads are similar for both analyses (Fig. 5 and Table 1). Because the loadings of short PC2 are opposite in sign to long PC2, we multiply the scores of the short window PC2 by −1 for equivalent comparison. Large loadings with opposite sign contributions for the 1123 and 607 benthic $\delta^{18}O_{sw}$ records suggest that PC2 represents differences in the $\delta^{18}O_{sw}$ of deep water in the Atlantic and Pacific basins. Most notably, PC2 has a strong peak at approximately

CPD
11, 3699–3728, 2015

250 ka (Fig. 5), associated with very low values in the 607 benthic $\delta^{18}O_{sw}$ record and very high values in the 1123 benthic $\delta^{18}O_{sw}$ record (Fig. 1).

PC3 captures 5 % of the variance in the 430 ka stack and 6 % of the variance in the 798 ka stack. Unlike PC1 and PC2, the loads vary between the short and long PC3 (Table 1); here we focus on the short version because it contains more proxy records. In the 430 ka stack, PC3 is most highly represented by the planktonic $\delta^{18}O_{sw}$ stack with a load of 0.7 and the 1123 and 607 benthic $\delta^{18}O_{sw}$ records with loads of about −0.4. These loads suggest that PC3 dominantly reflects planktonic vs. benthic differences in $\delta^{18}O_{sw}$. PC3 scores exhibit a linear trend from 0–430 ka, which supports the findings of previous studies that suggest planktonic $\delta^{18}O_{sw}$ should be detrended for conversion to sea level (Lea et al., 2002; Shakun et al., 2015). Furthermore, PC3 suggests that benthic $\delta^{18}O_{sw}$ may also need to be detrended in the opposite direction. This effect could be caused by long-term changes in the hydrologic cycle or deep water formation processes, which lead to a change in the partitioning of oxygen isotopes between the surface and deep ocean.

8 Conclusions

PCA indicates a strong common sea level signal in the seven records analyzed for 0–430 ka and five records for 0–798 ka. Furthermore, the similarity between the short and long stacks indicate that the longer stack with five records is nearly as good an approximation of sea level as the seven-record stack. Sea level estimates for each interglacial vary greatly between records, producing standard deviations of 11–26 m. Generally, the mean for each individual highstand is greater in magnitude than our stack estimate. Based on comparison with GIA-corrected coral sea level estimates for MIS 5e and 11, the stack likely reflects mean sea level for each interglacial and fails to capture brief sea level highstands, such as those lasting only ∼ 2 ka during MIS 5e.

CPD
11, 3699–3728, 2015

We estimate that sea level change accounts for only about 40 % of the orbital-band variance in benthic $\delta^{18}O_c$, compared to 65 % of the LGM-to-Holocene benthic $\delta^{18}O_c$ change. Nonetheless, benthic $\delta^{18}O_c$ is strongly correlated with sea level ($r = -0.9$). If LR04 benthic $\delta^{18}O_c$ stack is smoothed and lagged by 2 ka, the relationship between benthic $\delta^{18}O_c$ and sea level is well-described by a linear function from 398–798 ka and a quadratic function from 0–398 ka. In particular, interglacials MIS 9 and 5e which had larger ice sheets than MIS 11 appear to have been as warm (or warmer) than MIS 11 with isotopically less depleted ice sheets.

The second and third principal components of the sea level records describe differences between the proxies. PC2 represents the difference between the $\delta^{18}O_{sw}$ of deep water in the Atlantic and Pacific basins; a peak in PC2 scores at 250 ka indicates large differences between the basins at this time. PC3 represents the differences between planktonic and benthic $\delta^{18}O_{sw}$ records and suggests a linear trend between the two from 0–430 ka. Thus, $\delta^{18}O_{sw}$ records vary across ocean basins and between the surface and the deep. In conclusion, the stack of sea level proxies presented here should be a more accurate eustatic sea level record than any of the individual records it contains.

Data availability

The sea level stack is archived in the Supplement and (upon publication) at the World Data Center for Paleoclimatology operated by the National Climatic Data Center of the National Oceanographic and Atmospheric Association.

The Supplement related to this article is available online at doi:10.5194/cpd-11-3699-2015-supplement.

CPD
11, 3699–3728, 2015

Acknowledgements. We thank all researchers who made their data available. Additionally, we thank David Lea, Jeremy Shakun, Alex Simms, Charles Jones, and Leila Carvalho for beneficial discussions.

References

Adkins, J. F., McIntyre, K., and Schrag, D. P.: The salinity, temperature, and δ^{18}O of the glacial deep ocean, Science, 29, 1769–1773, doi:10.1126/science.1076252, 2002.

Bintanja, R., Roderik, S. W., and van de Wal, O. J.: Modeled atmospheric temperatures and global sea levels over the past million years, Nature, 437, 125–128, doi:10.1038/nature03975, 2005.

Clark, P. U., Dyke, A. S., Shakun, J. D., Carlson, A. E., Clark, J., Wohlfarth, B., Mitrovica, J. X., Hostetler, S. W., and McCabe, A. M.: The Last Glacial Maximum, Science, 325, 710–714, doi:10.1126/science.1172873, 2009.

Duplessy, J. C., Labeyrie, L., and Waelbroeck, C.: Constraints on the ocean isotopic enrichment between the Last Glacial Maximum and the Holocene: paleoceanographic implications, Quaternary Sci. Rev., 21, 315–330, 2002.

Elderfield, H., Ferretti, P., Greaves, M., Crowhurst, S. J., McCave, I. N., Hodell, D. A., and Piotrowski, A. M.: Evolution of ocean temperature and ice volume through the Mid-Pleistocene Climate Transition, Science, 337, 704–709, doi:10.1126/science.1221294, 2012.

Jouzel, J., Masson-Delmotte, V., Cattani, O., Dreyfus, G. Falourd, S., Hoffmann, G., Minster, B., Nouet, J., Barnola, J. M., Chappellaz, J., Fischer, H., Gallet, J. C., Johnsen, S., Leuenberger, M., Loulergue, L., Luethi, D., Oerter, H., Parrenin, F., Raisbeck, G., Raynaud, D., Schilt, A., Schwander, A., Selmo, E., Souchez, R., Spahni, R., Stauffer, B., Steffensen, J. P. Stenni, B., Stocker, T. F., Tison, J. L., Werner, M., and Wolff, E. W.: Orbital and millennial Antarctic climate variability over the past 800,000 years, Science, 317, 793, doi:10.1126/science.1141038, 2007.

Kopp, R. E., Simons, F. J., Mitrovica, J. X., Maloof, A. C., and Oppenheimer, M.: Probabilistic assessment of sea level during the last interglacial stage probabilistic assessment of sea level, Nature, 462, 863–867, doi:10.1038/nature08686, 2009.

CPD
11, 3699–3728, 2015

Kopp, R. E., Simons, F. J., Mitrovica, J. X., Maloof, A. C., and Oppenheimer, M.: A probabilistic assessment of sea level variations within the last interglacial stage, Geophys. J. Int., 193, 711–716, 2013.

Lambeck, K., Rouby, H., Purcell, A., Sun, Y., and Sambridge, M.: Sea level and global ice volumes from the Last Glacial Maximum to the Holocene, P. Natl. Acad. Sci. USA, 111, 43, doi:10.1073/pnas.1411762111, 2014.

Lisiecki, L. E. and Raymo, M. E.: A Pliocene-Pleistocene stack of 57 globally distributed benthic δ^{18}O records, Paleoceanography, 20, PA1003, doi:10.1029/2004PA001071, 2005.

Masson-Delmotte, V., Stenni, B., Jouzel, J., Landais, A., Röthlisberger, R., Minster, B., Hansen, J., Pol, K., Barnola, J. M., Mikolajewicz, U., Braconnot, P., Chappellaz, J., Otto-Bliesner, B., Cattani, O., and Krinner, G.: EPICA Dome C record of glacial and interglacial intensities, Quaternary Sci. Rev., 29, 113–128, 2010.

Medina-Elizalde, M.: A compilation of coral sea level benchmarks: implications and new challenges, Earth Planet. Sc. Lett., 362, 310–318, 2013.

Petit, J. R., Jouzel, J., Raynaud, D., Barkov, N. I., Barnola, J.-M., Basile, I., Bender, M., Chappellaz, J., Davisk, M., Delaygue, G., Delmotte, M., Kotlyakov, V. M., Legrand, M., Lipenkov, V. Y., Lorius, C., Pépin, L., Ritz, C., Saltzman, E., and Stievenard, M.: Climate and atmospheric history of the past 420,000 years from the Vostok ice core, Antarctica, Nature, 399, 429–436, 1999.

Raymo, M. E. and Mitrovica, J. X.: Collapse of polar ice sheets during the stage 11 interglacial, Nature, 483, 453–456, doi:10.1038/nature10891, 2012.

Raymo, M. E., Ruddiman, W. F., Shackleton, N. J., and Oppo, D. W.: Evolution of Atlantic–Pacific δ^{13}C gradients over the last 2.5 m.y., Earth Planet. Sc. Lett., 97, 353–368, 1990.

Rohling, E. J., Grant, K., Bolshaw, M., Roberts, A. P., Siddall, M., Hemleben, C., and Kucera, M.: Antarctic temperature and global sea level closely coupled over the past five glacial cycles, Nat. Geosci., 2, 500–504, 2009.

Rohling, E. J., Grant, K. M., Bolshaw, M., Roberts, A. P., Siddall, M., Hemleben, C., Kucera, M., Foster, G. L., Marino, G., Roberts, A. P., Tamisiea, M. E., and Williams, F.: Sea-level and deep-sea-temperature variability over the past 5.3 million years, Nature, 508, 477–482, 2014.

Schiebel, R., Zeltner, A., Treppke, U. F., Waniek, J. J., Bollmann, J., Rixen, T., and Hemleben, C.: Distribution of diatoms, coccolithophores and planktic foraminifera in the Arabian Sea, Mar. Micropaleontol., 51, 345–371, doi:10.1016/j.marmicro.2004.02.001, 2004.

CPD
11, 3699–3728, 2015

Shackleton, N. J.: Attainment of isotopic equilibrium between ocean water and the benthonic *foraminifera genus Uvigerina*: isotopic changes in the ocean during the last glacial, Colloque International sur les Methodes Quantitatives d'Etude des Variation du Climat au Sours du Pleistocene, Coll. Int. C.N.R.S., 219, 203–209, 1974.

Shakun, J. D., Clark, P. U., He, F., Marcott, S. A., Mix, A. C., Liu, Z., Otto-Bliesner, B., Schmittner, A., and Bard, E.: Global warming preceded by increasing carbon dioxide concentrations during the last deglaciation, Nature, 484, 49–54, doi:10.1038/nature10915, 2012.

Shakun, J. D., Lea, D. W., Lisiecki, L. E., and Raymo, M. E.: An 800-kyr record of global surface ocean $\delta^{18}O$ and implications for ice volume-temperature coupling, Earth Planet. Sc. Lett., 426, 58–68, 2015.

Siddall, M., Smeed, D. A., Hemleben, C., Rohling, E. J., Schmeltzer, I., and Peltier, W. R.: Understanding the Red Sea response to sea level, Earth Planet. Sc. Lett., 225, 421–434, 2004.

Sosdian, S. and Rosenthal, Y.: Deep-sea temperature and ice volume changes across the Pliocene-Pleistocene climate transitions, Science, 17, 306–310, doi:10.1126/science.1169938, 2009.

Tian, L., Yao, T., Schuster, P. F., White, J. W. C., Ichiyanagi, K., Pendall, E., Pu, J., and Yu, W.: Oxygen-18 concentrations in recent precipitation and ice cores on the Tibetan Plateau, J. Geophys. Res., 108, 4293, doi:10.1029/2002JD002173, 2003.

Thompson, W. G. and Goldstein, S. L.: Open-system coral ages reveal persistent suborbital sea-level cycles, Science, 308, 401–404, doi:10.1126/science.1104035, 2005.

Waelbroeck, C., Labeyrie, L., Michel, E., Duplessy, J. C., and McManus, J.: Sea-level and deep water temperature changes derived from benthic foraminifera isotopic records, Quaternary Sci. Rev., 21, 295–305, 2002.

CPD
11, 3699–3728, 2015

Table 1. Principal Component Analysis (PCA) loading for each proxy record. "Short" refers to the 0–430 ka time window, and "Long" refers to 0–798 ka. Numbers in parentheses give the percent variance explained by each principal component.

	PC1 Short (82 %)	PC1 Long (76 %)	PC2 Short (6 %)	PC2 Long (8 %)	PC3 Short (5 %)	PC3 Long (6 %)
Inverse model (Bintanja et al., 2005)	0.39	0.48	0.05	0.10	0.14	−0.02
Atl. benthic $\delta^{18}O_{sw}$ (Elderfield et al., 2012)	0.34	0.43	0.70	0.49	−0.44	−0.34
Planktonic $\delta^{18}O_{sw}$ (Shakun et al., 2015)	0.36	0.44	0.00	0.18	0.73	0.82
RSL_{Med} (Rohling et al., 2014)	0.38	0.44	0.01	0.08	−0.2	−0.42
Pac. benthic $\delta^{18}O_{sw}$ (Sosdian and Rosenthal, 2009)	0.34	0.42	−0.70	−0.84	−0.44	−0.02
$\delta^{18}O_c$ regression (Waelbroeck et al., 2002)	0.40	–	−0.08	–	0.09	–
RSL_{Red} (Rohling et al., 2009)	0.40	–	0.01	–	0.05	–

CPD
11, 3699–3728, 2015

Table 2. Sea level lowstand estimates (in meters above modern).

Marine Isotope Stage	2	10	12	16
Age Range (ka)	18–25	342–353	427–458	625–636
Inverse model (Bintanja et al., 2005)	−123	−111	−126	−126
Atl. benthic $\delta^{18}O_{sw}$ (Elderfield et al., 2012)	−113	−96	−146	−113
RSL_{Red} (Rohling et al., 2009)	−114	−114	−118	
RSL_{Med} (Rohling et al., 2014)	−120	−77		
Plank. $\delta^{18}O_{sw}$ (Shakun et al., 2015)	−130	−96	−143	−145
Pac. benthic $\delta^{18}O_{sw}$ (Sosdian and Rosenthal, 2009)	−124	−112	−100	−125
$\delta^{18}O_c$ regression (Waelbroeck et al., 2002)	−123	−126		
Standard deviation	5.9	16	19	13
Mean	−121	−105	−127	−127
Scaled PC1 (0–430 ka)	−130	−108		
Scaled PC1 (0–798 ka)	−130	−103	−119	−108
GIA-corrected corals (Clark et al., 2009; Lambeck et al., 2014)	−130 to −134			

CPD
11, 3699–3728, 2015

Table 3. Sea level highstand estimates (in meters above modern).

Marine Isotope Stage	5e	7a	7c	9	11	13	17	19
Age Range (ka)	119–126	197–214	236–255	315–331	399–408	486–502	682–697	761–782
Inverse model (Bintanja et al., 2005)	0.4	−20	−18	−0.5	0.2	−29	−23	−21
Atl. benthic $\delta^{18}O_{sw}$ (Elderfield et al., 2012)	3.3	12	16	40	58	18	31	21
RSL_{Red} (Rohling et al., 2009)	18	14	−3.2	11	3.5			
RSL_{Med} (Rohling et al., 2014)	−4.2	12	0.6	−5.3	12	−7.7	0.5	7.2
Plank. $\delta^{18}O_{sw}$ (Shakun et al., 2015)	−1.1	−6.7	−10	−18	3.9	−1.3	−2.5	12
Pac. benthic $\delta^{18}O_{sw}$ (Sosdian and Rosenthal, 2009)	28	34	−6.2	43	57	32	8.1	−6.8
$\delta^{18}O_c$ regression (Waelbroeck et al., 2002)	4.9	−3.6	−9.4	4.7	5.7			
Standard deviation	12	18	11	23	26	24	20	17
Mean	7.0	6.0	−4.3	11	20	2.4	2.8	2.5
Scaled PC1 (0–430 ka)	3.1	−7	−9.4	−0.6	16			
Scaled PC1 (0–798 ka)	−0.6	−4.9	−12.8	−2.3	19	−10.8	−9.1	−6.3
Coral 95 % confidence interval (Medina-Elizalde, 2013)	−1 to 4	−17 to 7	−19 to 11					
GIA-corrected corals (Kopp et al., 2009; Raymo and Mitrovica, 2013)	8 to 9.4				6 to 13			

CPD
11, 3699–3728, 2015

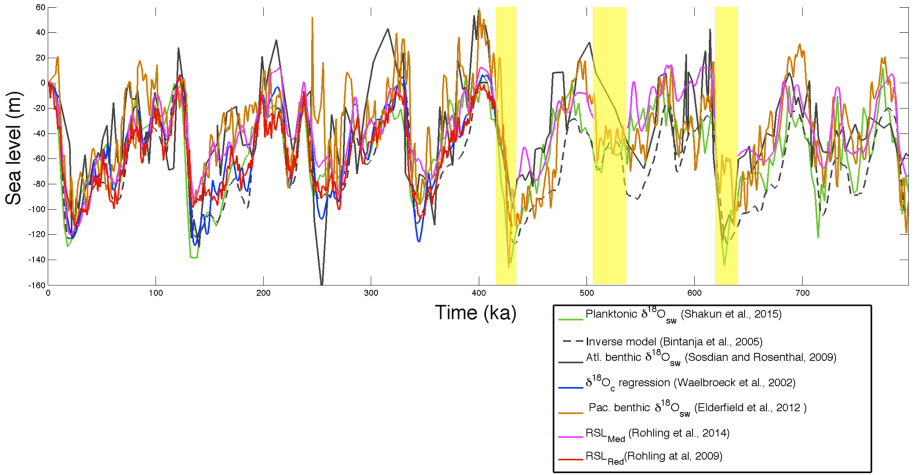

Figure 1. Eustatic and relative sea level estimates for the seven records on the LR04 age model (Lisiecki and Raymo, 2005). Yellow bars mark the sapropel layers removed from the Mediterranean RSL record (Rohling et al., 2014). Red Sea RSL (Rohling et al., 2009) is shown interpolated to 1 kyr spacing.

CPD
11, 3699–3728, 2015

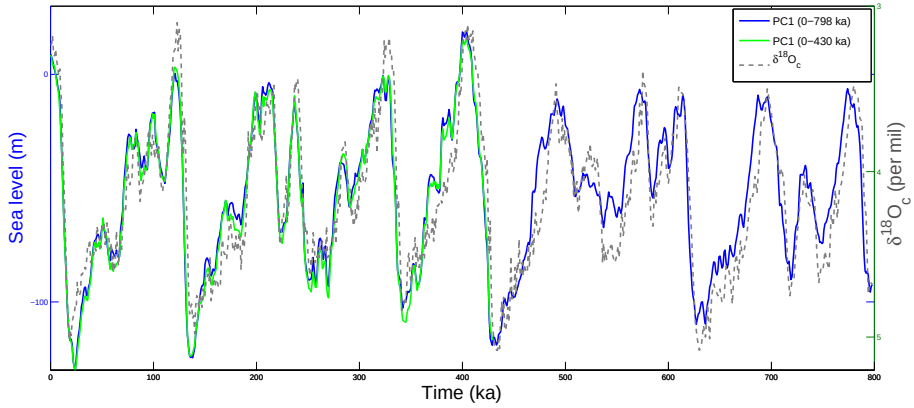

Figure 2. Long and short sea level stacks compared to the LR04 benthic $\delta^{18}O_c$ stack (Lisiecki and Raymo, 2005).

CPD
11, 3699–3728, 2015

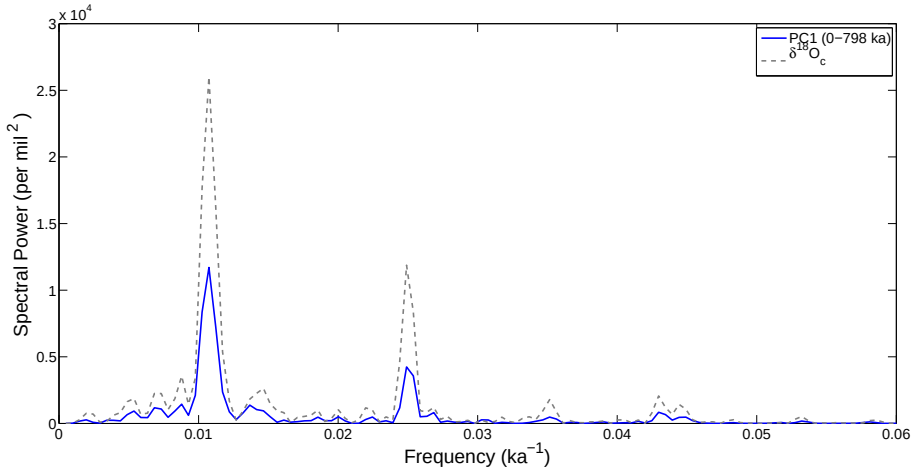

Figure 3. Spectral analysis for composite sea level stack converted to its $\delta^{18}O_{sw}$ contribution using 0.009 ‰ m^{-1} and benthic $\delta^{18}O_c$ stack (Lisiecki and Raymo, 2005) from 0–798 ka.

CPD
11, 3699–3728, 2015

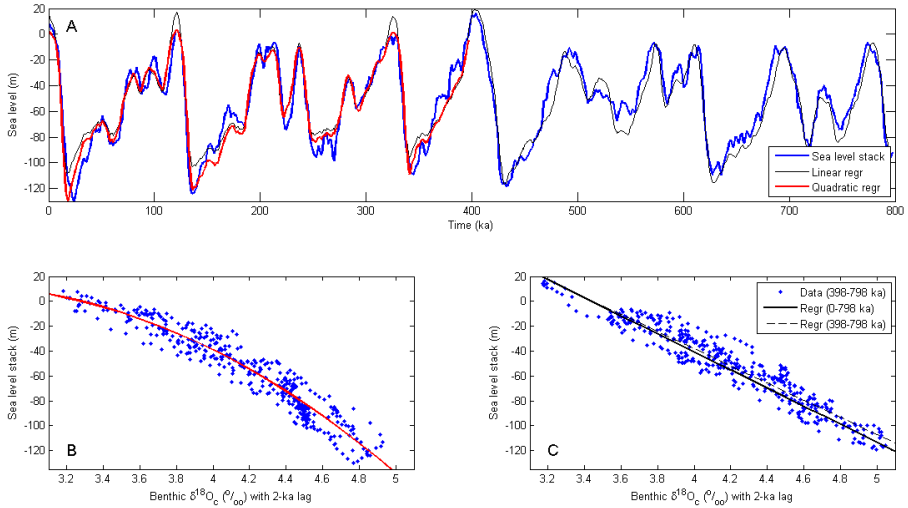

Figure 4. Comparison of benthic $\delta^{18}O_c$ and sea level. **(a)** Linear and quadratic sea level models (Eqs. 1 and 2, respectively) using smoothed benthic $\delta^{18}O_c$ lagged by 2 ka (Lisiecki and Raymo, 2004). **(b)** Time window 0–397 ka with quadratic regression (red line). **(c)** Time window 398–798 ka with linear regression for 0–798 and 398–798 ka.

CPD
11, 3699–3728, 2015

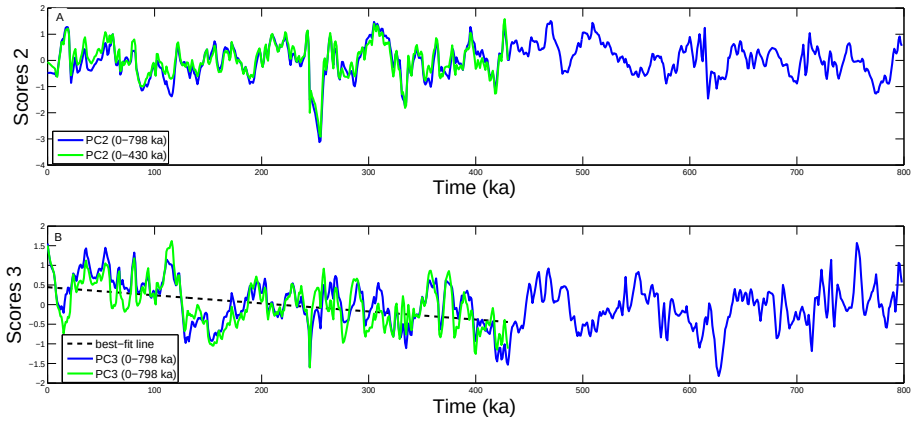

Figure 5. Second and third principal components for 0–430 ka and 0–798 ka. **(a)** Scores for PC2 largely reflect difference between Atlantic and Pacific benthic $\delta^{18}O_{sw}$. **(b)** Scores for PC3. Dashed black line marks linear trend from 0–430 ka.

CPD
11, 3699–3728, 2015